


# Autofluorescence pattern of parathyroid adenomas

M. S. Demarchi <sup>1,\*</sup>, W. Karenovics<sup>1</sup>, B. Bédât<sup>1</sup>, C. De Vito<sup>2</sup> and F. Triponez<sup>1,\*</sup>

<sup>1</sup>Department of Thoracic and Endocrine Surgery and Faculty of Medicine, University Hospitals of Geneva, Geneva, Switzerland

<sup>2</sup>Division of Clinical Pathology, Geneva University Hospitals, Geneva, Switzerland

\*Correspondence to: (F.T.) Department of Thoracic and Endocrine Surgery and Faculty of Medicine, University Hospitals of Geneva, 4 Rue Gabrielle Perret-Gentil, 1211 Geneva (e-mail: frederic.triponez@hcuge.ch); (M.S.D.) Department of Thoracic and Endocrine Surgery and Faculty of Medicine, University Hospitals of Geneva, 4 Rue Gabrielle Perret-Gentil, 1211 Geneva, Switzerland (e-mail: marcostefano.demarchi@hcuge.ch)

## Abstract

**Background:** Primary hyperparathyroidism (pHPT) is a common endocrine pathology, and it is due to a single parathyroid adenoma in 80–85 per cent of patients. Near-infrared autofluorescence (NIRAF) has recently been used in endocrine surgery to help in the identification of parathyroid tissue, although there is currently no consensus on whether this technique can differentiate between normal and abnormal parathyroid glands. The aim of this study was to describe the autofluorescence pattern of parathyroid adenoma in pHPT.

**Methods:** Between January and June 2019, patients with pHPT who underwent surgical treatment for parathyroid adenoma were enrolled. Parathyroid autofluorescence was measured.

**Results:** Twenty-three patients with histologically confirmed parathyroid adenomas were included. Parathyroid adenomas showed a heterogeneous fluorescence pattern, and a well defined autofluorescent ‘cap’ region was observed in 17 of 23 specimens. This region was on average 28 per cent more fluorescent than the rest of the adenoma, and corresponded to a rim of normal histological parathyroid tissue (sensitivity and specificity 88 and 67 per cent respectively). After resection, all patients were treated successfully, with normal postoperative values of calcium and parathyroid hormone documented.

**Conclusion:** Parathyroid adenomas show a heterogeneous autofluorescence pattern. Using NIRAF imaging, the majority of specimens showed a well defined autofluorescent portion corresponding to a rim of normal parathyroid tissue. Further studies should be conducted to validate these findings.

## Introduction

Primary hyperparathyroidism (pHPT) is a frequent endocrine pathology that affects 0.3 per cent of the general population, and results from the inappropriate production of parathyroid hormone (PTH) from one or more parathyroid glands<sup>1</sup>. This condition is linked to single parathyroid adenoma in 80–85 per cent of patients<sup>2</sup>. Surgery has been widely recognized as the standard treatment in the management of pHPT<sup>3</sup>, which has led to the development of minimally invasive surgical procedures<sup>4,5</sup>. Different imaging modalities, such as ultrasonography and <sup>99m</sup>Tc-labelled sestamibi (sestamibi) scintigraphy, have been used to identify and localize diseased parathyroid tissue before surgery, with sensitivities of 69–75 and 49–70 per cent respectively<sup>6,7</sup>. Other emerging techniques, such as multiphase four-dimensional CT and <sup>18</sup>F-labelled choline PET-CT, are increasingly being used to facilitate accurate preoperative localization, particularly in the setting of negative or discordant ultrasonography and sestamibi imaging<sup>8,9</sup>.

In some centres, intraoperative PTH testing is used after excision to confirm that the correct parathyroid adenoma has been removed adequately, which offers the benefits of

minimizing the extent of surgical dissection and rate of persistence/recurrence<sup>3</sup>.

Despite significant advances in imaging, intraoperative detection of normal and abnormal parathyroid glands remains a major challenge for both expert and non-expert endocrine surgeons<sup>10</sup>. A novel imaging modality that uses near-infrared autofluorescence (NIRAF) has recently been described for the intraoperative localization of normal parathyroid glands<sup>11–15</sup>; however, whether NIRAF can be used to differentiate between hyperfunctioning and normal functioning parathyroid tissue remains unclear, with inconsistent results published across studies<sup>16,17</sup>.

The purpose of this study was to describe the autofluorescence patterns exhibited by hyperfunctioning parathyroid tissue in patients with pHPT undergoing parathyroidectomy, and to explore associations between NIRAF patterns and histopathological findings.

## Methods

Patients with a confirmed diagnosis of pHPT who underwent parathyroidectomy at Geneva University Hospital between January and June 2019 were reviewed retrospectively. The

Received: April 29, 2020. Revised: October 11, 2020. Accepted: November 05, 2020

© The Author(s) 2021. Published by Oxford University Press on behalf of BJS Society Ltd.

This is an Open Access article distributed under the terms of the Creative Commons Attribution Non-Commercial License (<http://creativecommons.org/licenses/by-nc/4.0/>), which permits non-commercial re-use, distribution, and reproduction in any medium, provided the original work is properly cited. For commercial re-use, please contact [journals.permissions@oup.com](mailto:journals.permissions@oup.com)

patients included were aged over 18 years, and were diagnosed with pHPT using laboratory and preoperative imaging studies. Patients with secondary or tertiary hyperparathyroidism were excluded.

For each patient, the following data were recorded: medical history, demographic characteristics, preoperative laboratory evaluation (serum calcium and PTH levels), and results of imaging studies (including ultrasound examination, sestamibi scintigraphy, and  $^{18}\text{F}$ -labelled choline PET-CT, when performed). Samples were also collected for measurement of serum calcium and PTH levels 4 h after surgery, and on postoperative days 1 and 10. Calcium and PTH were measured at the Central Clinical Laboratory of the Geneva University Hospital.

This study was approved by the Institutional Review Board of Geneva University Hospitals, and all subjects signed written consent before enrolment.

### Surgical treatment and autofluorescence

All operations were performed by an experienced endocrine surgeon using the typical standard of care in a high-volume hospital. Unilateral neck exploration was chosen for adenomas that had been clearly localized before operation, whereas bilateral neck exploration was performed in patients with discordant or inconclusive preoperative imaging findings or multiple lesions. All patients underwent parathyroidectomy for pHPT using autofluorescence imaging. A Fluobeam LX<sup>®</sup> device (Fluoptics, Grenoble, France) was used to capture intraoperative and resected specimen images.

During surgery, the Fluobeam LX<sup>®</sup> device was used to help in the identification of parathyroid glands (Fig. 1). Once the parathyroidectomy had been completed, the resected specimen was exposed to near-infrared light, and the resulting fluorescence was captured using the same device held at a distance of 20 cm from the specimen, under the same ambient light as that used in the operating room (Figs 2 and 3).

The NIRAF images were analysed using ImageJ software (National Institutes of Health, Bethesda, Maryland USA)<sup>18</sup>. The autofluorescence patterns observed visually were classified as either homogeneous, when the adenoma fluorescence detected by the device was uniform, or heterogeneous, when a mixture of

bright and dim areas was recorded. The presence of a single well defined bright autofluorescent region was defined as the 'cap' (Fig. 2), and indicated with a surgical marker for pathological assessment (Fig. 4 and Video S1); of note, the ink emits a reproducible standardized fluorescence signal.

Variables collected from the NIRAF image of the resected specimens included the size of the area resected, the mean fluorescence measurements for the whole adenoma, and both the brightest (most autofluorescent) and dimmest regions of the resected specimen, which were used to calculate the fluorescence score. This score was created to normalize and establish uniformity among the measurements, and was calculated by dividing the mean fluorescence intensity for the three measurements by the mean fluorescence intensity of the same  $1 \times 1\text{-cm}$ -square region marked on a white surgical ruler with the purple surgical marker used for marking the surgical specimen (Fig. 5).

The resected specimens were then transferred to the pathology department of the University of Geneva for histological analysis, including the marked and unmarked areas of the specimen.

### Statistical analysis

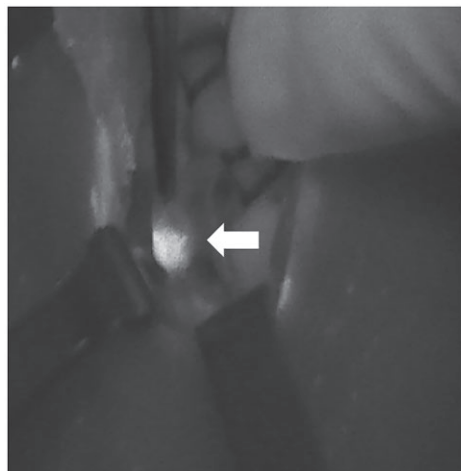
Continuous variables are expressed as mean(SD). Statistical analysis was performed using XLSTAT (Addinsoft, PARIS, France) for Excel<sup>™</sup> (Microsoft, Redmond, Washington, USA). Student's *t* test was used to test the statistical significance of differences and  $P < 0.050$  was considered statistically significant.

### Results

Of 29 patients who underwent parathyroidectomy during the study interval, 23 were selected according to the study criteria.

All included patients underwent parathyroid adenoma resection for pHPT (mean(SD) preoperative PTH 13.65(6.31) pmol/l); however, two of these patients also underwent thyroid lobectomy because of the simultaneous presence of thyroid disease. The adenoma was confirmed and localized before surgery by both ultrasonography and sestamibi scintigraphy in 18 patients. The adenoma was detected only by sestamibi scintigraphy in three patients, and by neither of these modalities in two. Finally, four patients were investigated using  $^{18}\text{F}$ -labelled choline PET-CT.

**a** Parathyroid adenoma



**b** Normal parathyroid glands

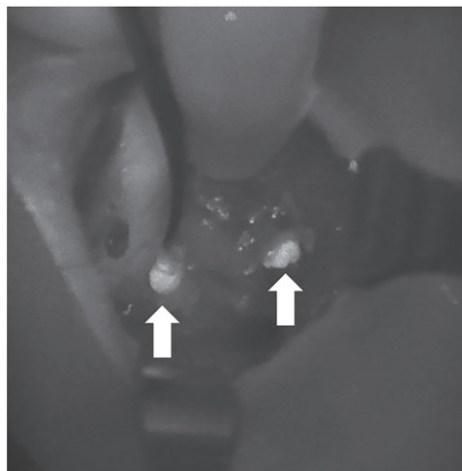


**Fig. 1** Intraoperative images captured with Fluobeam LX<sup>®</sup> device

Near-infrared autofluorescence image of **a** parathyroid adenoma and **b** two normal parathyroid glands.

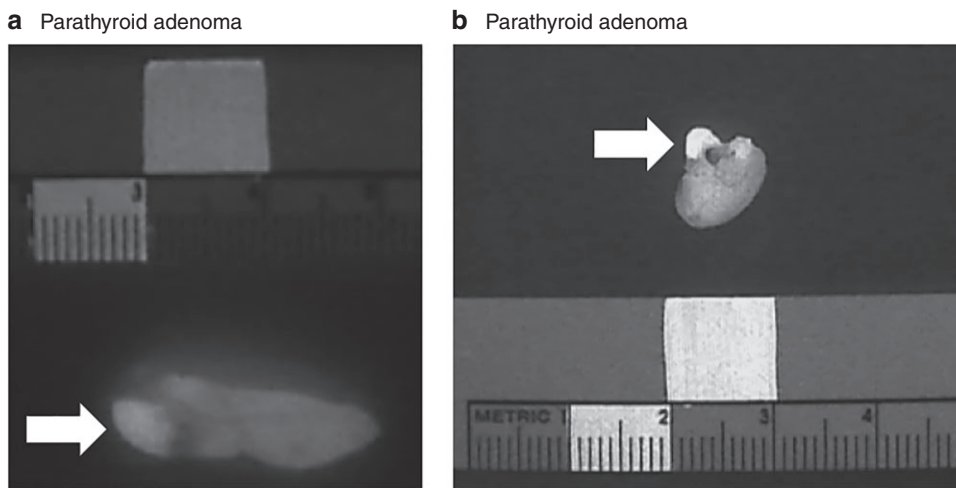


**Fig. 2** Near-infrared autofluorescence images captured after resection of parathyroid adenomas

**a,b** Images show the heterogeneous dim autofluorescence pattern of two adenomas; the brighter and more intense autofluorescence signal of a cap is highlighted by arrows. In both images, a  $1 \times 1$ -cm-square is indicated on a surgical ruler (in colour, the marking is purple on a white ruler). To calculate the fluorescence score (see text), the values were normalized based on the mean fluorescence intensity of the  $1 \times 1$ -cm square to overcome differences in image exposure.

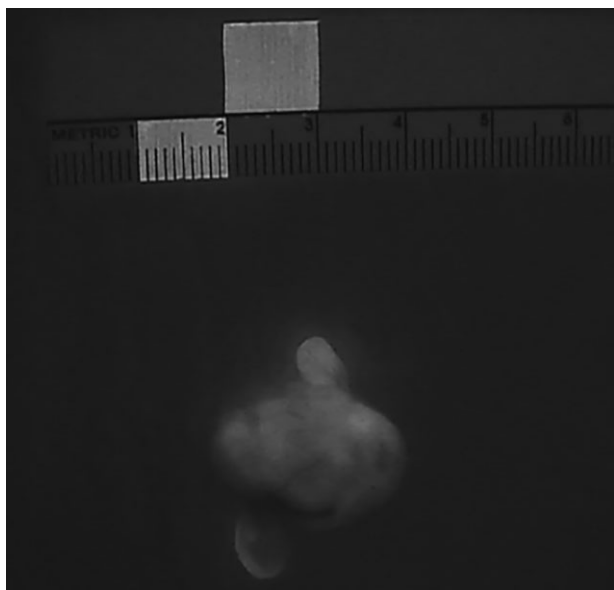


**Fig. 3** Near-infrared autofluorescence image captured after resection of a parathyroid adenoma

Image shows the heterogeneous autofluorescence pattern of the adenoma and absence of the cap. A  $1 \times 1$ -cm square is indicated on a surgical ruler (in colour, the marking is purple on a white ruler) at the top of the image.

Patient demographics, clinical characteristics, and interventions are summarized in [Table 1](#). The median age of the cohort was 56 (range 40–83) and median BMI was 25.1 (18–35)  $\text{kg}/\text{m}^2$ . Preoperative and postoperative serum calcium and PTH levels are shown in [Table S1](#). A single parathyroid adenoma was resected in 22 patients, and two adenomas were resected in one patient, who underwent bilateral cervical exploration; this was based on negative preoperative localization studies and intraoperative finding of increased size of the two parathyroid glands (intraoperative PTH measurement is not performed routinely in this institution) ([Fig. 6](#)).

All patients were treated successfully, and had normal calcium (2.42(0.15)  $\text{mmol}/\text{l}$ ) and PTH (1.87(0.84)  $\text{pmol}/\text{l}$ ) values on postoperative day 1, and 10 days after the intervention (calcium 2.32(0.11)  $\text{mmol}/\text{l}$ ; PTH 3.65(1.13)  $\text{pmol}/\text{l}$ ) ([Table S1](#)). The pathological reports confirmed the diagnosis of parathyroid adenoma.

### Fluorescence pattern

All adenomas showed a heterogeneous pattern of autofluorescence. Adenomas in 17 of the 23 patients exhibited a cap region, showing a clear, well defined bright autofluorescent region within the gland ([Fig. 2](#)). The remaining six patients had either low or heterogeneous signals ([Fig. 3](#)). Specifically, in two patients the adenomas displayed a very low heterogeneous signal and did not have an appreciably more autofluorescent part, so were not marked ([Fig. 7](#)); on the other hand, the remaining four adenomas had an autofluorescent region, although this was not sufficiently bright to be defined as a cap.

The difference in mean enhancement of fluorescence scores between the most and least fluorescent regions was 1.51(0.65) fold ([Table 2](#)); this corresponded to a mean 28 per cent in difference fluorescence intensity ([Fig. 8](#)). On the other hand, normal parathyroid tissue, documented on histopathological examination, had a 1.39(0.2)-fold (27 per cent) higher NIRAF signal compared with adenomas.

Of note, the fold increase between fluorescence scores was 1.59(0.73) (31 per cent mean difference) for adenomas presenting with a cap and 1.26(0.17) (19 per cent mean difference) for those without a cap.

The performance of the cap in detecting normal parathyroid tissue in a suspected adenomatous parathyroid was assessed ([Table 3](#)). Presence of a cap could detect normal parathyroid tissue in a parathyroid adenoma with a sensitivity of 88 per cent and a specificity of 67 per cent.

### Histological analysis

Histological findings are summarized [Table 4](#). Briefly, all resected specimens fulfilled the criteria for diagnosis of parathyroid adenoma. In 17 of 21 specimens marked by the surgeon following the NIRAF evaluation, a rim of normal parathyroid was observed

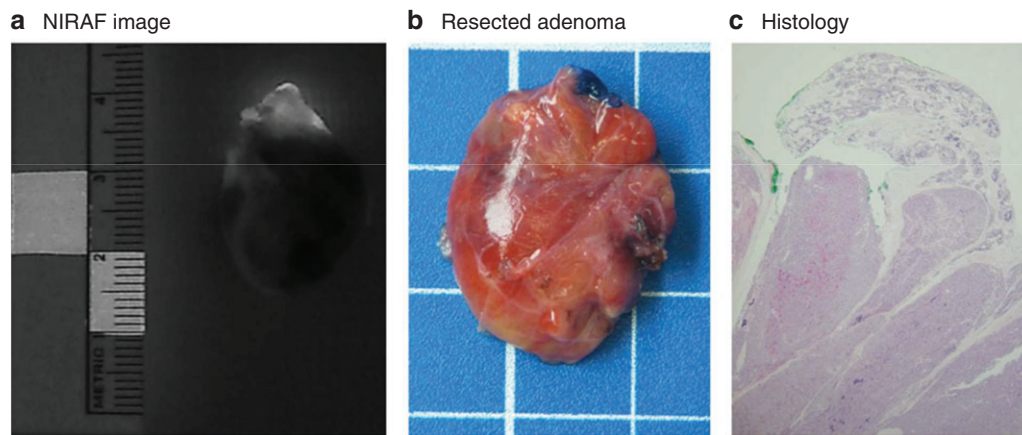


**Fig. 4** Near-infrared autofluorescence image, operative specimen, and histology of parathyroid adenoma

**a** Near-infrared autofluorescence (NIRAF) image showing cap of parathyroid adenoma; **b** surgical specimen showing cap marked with surgical ink; and **c** histological analysis showing a conserved rim of normal parathyroid tissue (green ink) corresponding to the marked area in **b** (haematoxylin and eosin stain; original magnification  $\times 20$ ).

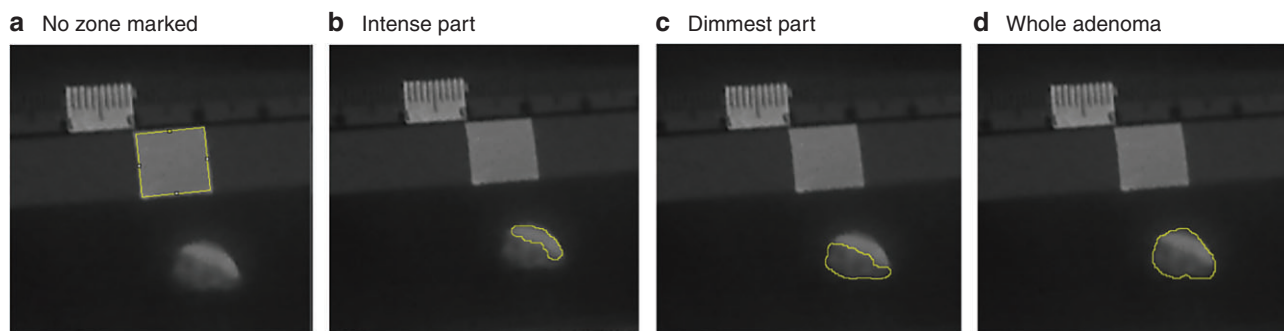


**Fig. 5** Zones of fluorescence intensity

Zones of fluorescence intensity detected with ImageJ software are outlined in yellow: **a** no zone marked; **b** most intense part of resected specimen (cap); **c** dimmest part of resected specimen; and **d** whole adenoma. A 1 × 1-cm-square is indicated on a surgical ruler (in colour, the marking is purple on a white ruler).

**Table 1** Patient characteristics, results of preoperative imaging, interventions, and resected gland(s)

Patient no.	Sex	BMI (kg/m <sup>2</sup> )	Age (years)	Ultrasound localization	Scintigraphy localization	Localization concordance	PET localization	Intervention	Resected gland
1	F	26.8	48	NO	NO	NO	NP	Bilateral exploration	SUP R
2	M	22.7	59	YES	YES	YES	NP	Unilateral parathyroidectomy	INF L
3	F	22.8	51	YES	YES	YES	NP	Unilateral parathyroidectomy and thyroid lobectomy	INF L
4	M	29	71	YES	YES	YES	NP	Unilateral parathyroidectomy	SUP L
5	F	26.1	45	YES	YES	YES	NP	Unilateral parathyroidectomy	INF R
6	F	19.9	52	NO	YES	NO	NP	Unilateral parathyroidectomy	INF L
7	F	30.1	43	YES	YES	YES	NP	Unilateral parathyroidectomy	INF L
8	F	18.1	56	YES	NO	NO	YES	Bilateral exploration	INF R
9	F	22.3	49	YES	YES	YES	NP	Unilateral parathyroidectomy	SUP R
10	F	28.6	54	YES	YES	YES	NP	Unilateral parathyroidectomy and thyroid lobectomy	SUP L
11	F	22.1	48	NO	YES	NO	NP	Unilateral parathyroidectomy	SUP R
12	F	26.9	75	YES	YES	YES	NP	Unilateral parathyroidectomy	INF R
13	F	35	55	YES	YES	YES	YES	Unilateral parathyroidectomy	INF L
14	F	22.5	55	YES	YES	YES	NP	Unilateral parathyroidectomy	INF L
15	F	25.4	40	YES	YES	YES	NP	Unilateral parathyroidectomy	SUP R
16	F	25.1	75	YES	NO	NO	YES	Bilateral exploration	INF L + SUP R
17	F	22.2	62	YES	YES	YES	NP	Unilateral parathyroidectomy	INF L
18	F	23.8	75	YES	YES	YES	NP	Unilateral parathyroidectomy	SUP R
19	M	28	63	NO	YES	NO	NP	Bilateral exploration	SUP L
20	F	18	83	YES	NO	NO	NP	Unilateral parathyroidectomy	SUP L
21	F	21	68	NO	YES	NO	NP	Unilateral parathyroidectomy	INF R
22	F	30	59	YES	YES	YES	NP	Unilateral parathyroidectomy	INF R
23	F	29	59	NO	NO	NO	YES	Unilateral parathyroidectomy	Ectopic SUP L

SUP, superior; INF, inferior; R, right; L, left; NP, not performed.

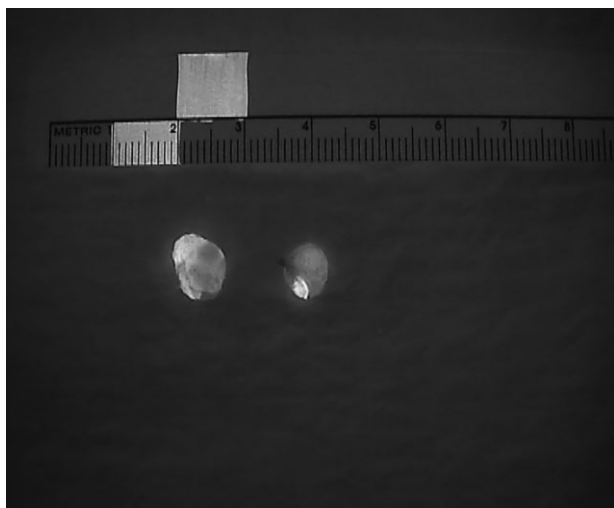


**Fig. 6** Near-infrared autofluorescence image of two different adenomas resected in the same patient

The specimen on the right has a cap, whereas that on the left has no clear cap but a well defined region of higher autofluorescence intensity.

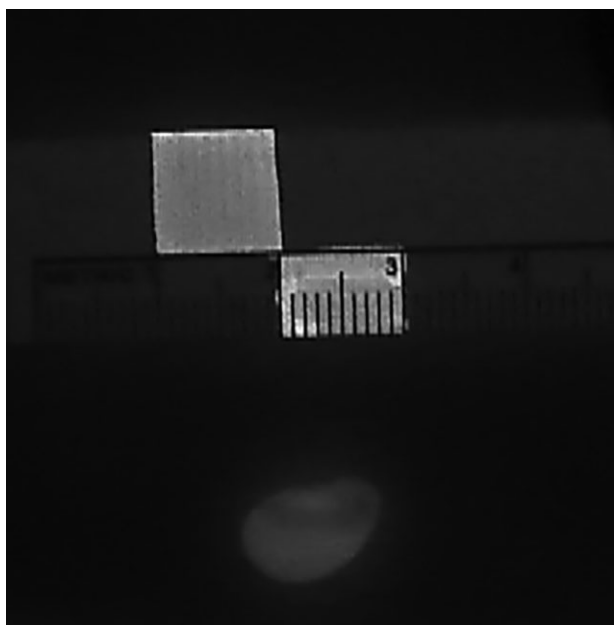


**Fig. 7** Near-infrared autofluorescence image of parathyroid adenoma with no clear cap or well defined region of higher intensity marked during surgery

(Fig. 4). Adipose tissue was noted in two instances, one with white and the other with brown adipose tissue (Figs 9 and 10), which is a well known cause of false-positive NIRAF findings in non-parathyroid tissues<sup>12,14,19</sup>. One specimen showed mild oncocyctic (oxyphilic) foci of the parathyroid adenoma, and in another the mark was wrongly placed on the adenomatous part of the specimen. In 15 of 17 specimens exhibiting a well defined more autofluorescent cap on NIRAF imaging, the rim of normal residual parathyroid tissue was marked correctly.

## Discussion

Localization of parathyroid glands during parathyroidectomy remains one of the major challenges faced by endocrine surgeons, who must otherwise rely on visual assessment to identify the gland. Frozen-section analysis and intraoperative parathyroid aspiration (and intraoperative PTH measurement of the aspirate) have been used to identify parathyroid tissue and confirm removal of the correct parathyroid gland<sup>20,21</sup>. However, there remains a clinical need for better identification of normal and diseased parathyroid glands, including instantaneous, intraoperative identification. Even with the use of preoperative imaging, such as ultrasound examination and MIBI scintigraphy which, when combined, are considered to be the most sensitive preoperative imaging examinations (sensitivity approximately 90 per cent)<sup>22</sup>, intraoperative localization of the diseased glands or adenoma with a high level of certainty is still difficult.

Paras and colleagues<sup>11</sup> first described the intrinsic autofluorescence properties of the parathyroid glands in the near-infrared range. This technique is based on the fact that, when parathyroid glands are stimulated by near infrared light (at about 780 nm), they re-emit significantly more autofluorescent light (at about 825 nm) than the surrounding tissues (such as thyroid, fat, vessels, lymph nodes), which enables their detection and identification by means of a label-free imaging system. A near-infrared autofluorescence signal has been used progressively in endocrine surgery for identification of parathyroid gland during thyroidectomy and parathyroidectomy, with the potential to provide real-time intraoperative feedback<sup>12,23</sup>.

Until now, discriminant traits in NIRAF signals between normal and abnormal parathyroid gland have not been demonstrated clearly, with conflicting results between authors. Therefore, no consensus exists regarding whether NIRAF imaging of parathyroid tissue can differentiate a normally functioning parathyroid gland from a diseased one<sup>14</sup>.

A previous study<sup>24</sup> found that diseased parathyroid glands show weaker NIRAF intensity than normal glands, and another<sup>16</sup> reported that hyperfunctioning parathyroid glands exhibit lower autofluorescence intensity than normally functioning glands. However, other studies<sup>25–26</sup> found no significant difference in NIRAF intensity between healthy and diseased parathyroid glands associated with pHPT, as later confirmed by further research<sup>27,28</sup>. Moreover, it has been reported that parathyroid adenomas in pHPT show higher NIRAF intensities than normal parathyroid glands<sup>29</sup>.

In the present study, most parathyroid adenomas demonstrated a heterogeneous NIRAF pattern, with adenoma tissue documented as significantly less autofluorescent than the rim of normal parathyroid tissue. It was also observed that parathyroid adenomas expressed on average approximately 28 per cent lower fluorescence intensity than the most intense region of the adenoma. However, the reason for the discrepancy regarding the autofluorescence signal in six samples remains unclear and requires further investigation, as the present study was limited in terms of the number of patients included.

NIRAF could therefore be a useful tool during parathyroidectomy, first to locate the normal and diseased parathyroid glands, and then to confirm that a parathyroid gland is indeed an adenoma when a cap of more autofluorescent tissue is found. Further studies should be conducted to validate these findings and the accuracy of this tool.

Table 2 Near-infrared autofluorescence image scores

Patient no.	Fluorescence score			Fold mean fluorescence		
	Greatest NIRAF signal	Lowest NIRAF signal	Fluorescence difference (%)	Greatest NIRAF signal	Lowest NIRAF signal	Fold change in mean fluorescence intensity
1	113	77	32	1.85	1.26	1.47
2	67	36	46	1.10	0.59	1.86
3	49	48	2	0.80	0.79	1.02
4	87	72	17	1.43	1.18	1.21
5	106	60	43	1.74	0.98	1.77
6	85	61	28	1.39	1.00	1.39
7	77	52	32	1.26	0.85	1.48
8	73	57	22	1.20	0.93	1.28
9	69	16	77	1.13	0.26	4.31
10	79	67	15	1.30	1.10	1.18
11	87	77	11	1.43	1.26	1.13
12	59	43	27	0.97	0.70	1.37
13	90	84	7	1.48	1.38	1.07
14	45	39	13	0.74	0.64	1.15
15	27	17	37	0.44	0.28	1.59
16	112	78	30	1.84	1.28	1.44
17	53	34	36	0.87	0.56	1.56
18	153	131	14	2.51	2.15	1.17
19	83	57	31	1.36	0.93	1.46
20	140	93	34	2.30	1.52	1.51
21	95	61	36	1.56	1.00	1.56
22	114	94	18	1.87	1.54	1.21
23	80	52	35	1.31	0.85	1.54
Mean(SD.)	84(29.6)	61(26.1)	28	1.38(0.49)	1.00(0.43)	1.51(0.65)

NIRAF, near-infrared autofluorescence scores were calculated as the normalized mean autofluorescence intensity in the most autofluorescent region (Fig. 5b) and the rest of the adenoma (Fig. 5c), with the difference in fluorescence expressed as a percentage and fold change.

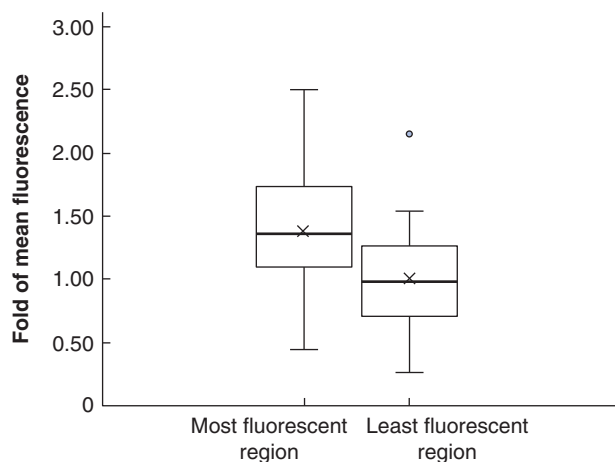


**Fig. 8** Fold of mean near-infrared autofluorescence differences between the most intense and dimmest parts of the resected specimen

Median (bold line), mean (cross), i.q.r. (box), and range (error bars) excluding outlier (circle) are shown.

**Table 3** Accuracy of detection of the cap on normal parathyroid tissue

	Normal parathyroid histology	
	Yes	No
Cap	15	2
No cap	2	4
Total	17	6

Sensitivity 88 (95 per cent c.i. 64 to 99) per cent, specificity 67 (22 to 96) per cent.

**Table 4** Histological findings in resected specimens and within ink-marked zone

Patient no.	Pathological findings on marked part	Cap	Dimension (mm)	Weight (g)
1	Ink: normal parathyroid	Yes	25	0.335
2	Ink: normal parathyroid	Yes	12	0.207
3	No ink	No	15	0.257
4	No ink	No	18	0.479
5	Ink: adipose tissue	Yes	20	0.729
6	Ink: normal parathyroid	Yes	11	0.200
7	Ink: adenoma, away from normal parathyroid	No	20	1.521
8	Ink: normal parathyroid	Yes	11	0.195
9	Ink: brown adipose tissue	Yes	3	2.290
10	Ink: mild oncocytic metaplasia	No	2	0.823
11	Ink: normal parathyroid	Yes	17	0.187
12	Ink: normal parathyroid	Yes	25	1.950
13	Ink: normal parathyroid	Yes	25	1.710
14	Ink: normal parathyroid	Yes	15	0.495
15	Ink: normal parathyroid	Yes	30	2.064
16	Ink: normal parathyroid	Yes	10	0.220
17	Ink: normal parathyroid	Yes	15	0.247
18	Ink: normal parathyroid	Yes	16	0.168
19	Ink: normal parathyroid	No	19	1.492
20	Ink: normal parathyroid	Yes	14	0.208
21	Ink: normal parathyroid	Yes	14	0.169
22	Ink: normal parathyroid	No	20	1.020
23	Ink: normal parathyroid	Yes	17	0.308

Disclosure. The authors declare no conflict of interest.

## Supplementary material

Supplementary material is available at BJS Open online.

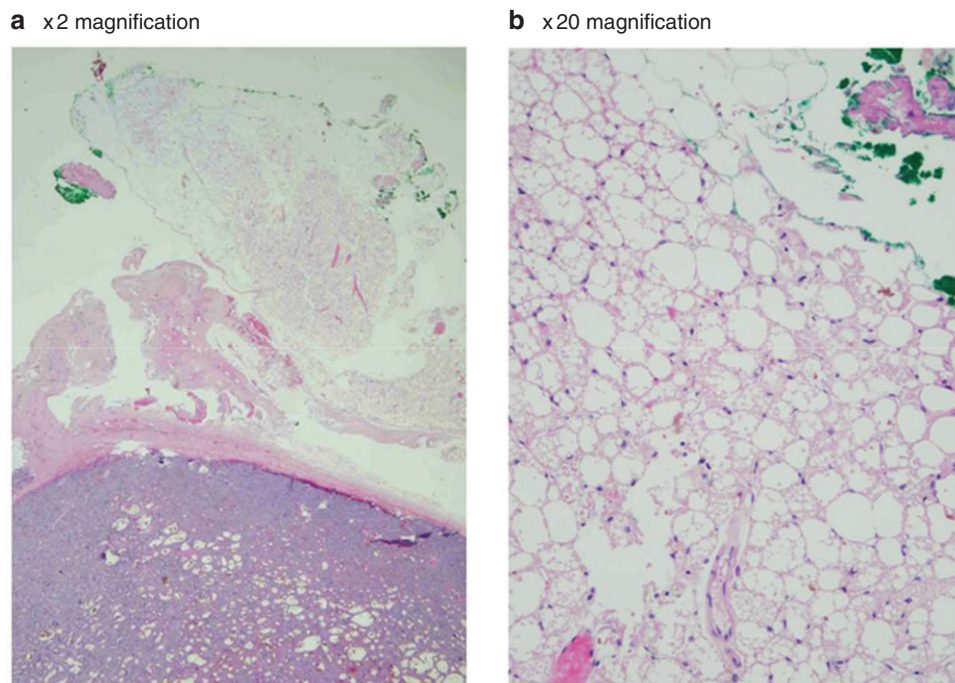


**Fig. 9 Parathyroid adenoma with brown adipose tissue**

Brown adipose tissue is marked with green ink (haematoxylin and eosin stain; original magnification **a**  $\times 20$ , **b**  $\times 200$ ).

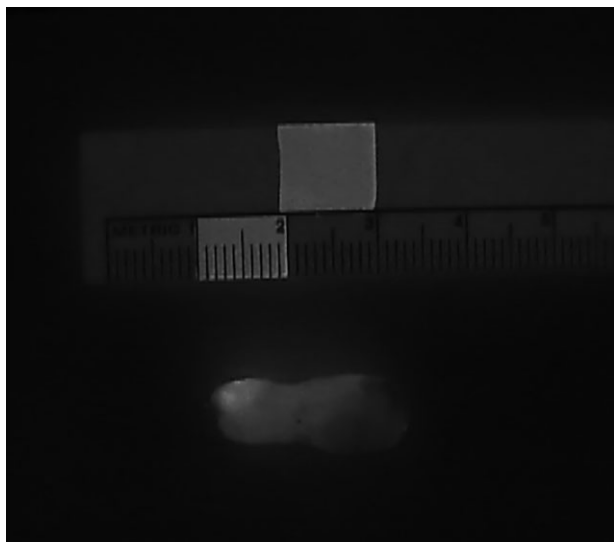


**Fig. 10 Near-infrared false-positive autofluorescence image of a parathyroid adenoma, which was confirmed as adipose tissue on anatomopathological analysis**

## References

1. Bilezikian JP, Bandeira L, Khan A, Cusano NE. Hyperparathyroidism. *Lancet* 2018;**391**:168–178
2. MacKenzie-Feder J, Sirrs S, Anderson D, Sharif J, Khan A. Primary Hyperparathyroidism: an Overview. *Int J Endocrinol* 2011;**2011**:1–8
3. Wilhelm SM, Wang TS, Ruan DT, Lee JA, Asa SL, Duh QY et al. The American Association of Endocrine Surgeons guidelines for definitive management of primary hyperparathyroidism. *JAMA Surg* 2016;**151**:959–968
4. Mollerup CL, Vestergaard P, Frøkjær VG, Mosekilde L, Christiansen P, Blichert-Toft M et al. Risk of renal stone events in primary hyperparathyroidism before and after parathyroid surgery: controlled retrospective follow up study. *BMJ* 2002;**325**:807–807
5. Silverberg SJ, Shane E, Jacobs TP, Siris E, Bilezikian JP. A 10-year prospective study of primary hyperparathyroidism with or without parathyroid surgery. *N Engl J Med* 1999;**341**:1249–1255
6. Siperstein A, Berber E, Barbosa GF, Tsinberg M, Greene AB, Mitchell J et al. Predicting the success of limited exploration for primary hyperparathyroidism using ultrasound, sestamibi, and intraoperative parathyroid hormone: analysis of 1158 cases. *Ann Surg* 2008;**248**:420
7. Kim SW, Lee HS, Lee KD. Intraoperative real-time localization of parathyroid gland with near infrared fluorescence imaging. *Gland Surg* 2017;**6**:516–524
8. Bunch PM, Kelly HR. Preoperative imaging techniques in primary hyperparathyroidism: a review. *JAMA Otolaryngol Head Neck Surg* 2018;**144**:929–937
9. Beheshti M, Hehenwarter L, Paymani Z, Rendl G, Imamovic L, Rettenbacher R et al.  $^{18}\text{F}$ -fluorocholine PET/CT in the assessment of primary hyperparathyroidism compared with  $^{99\text{m}}\text{Tc}$ -MIBI or  $^{99\text{m}}\text{Tc}$ -tetrofosmin SPECT/CT: a prospective dual-centre study in 100 patients. *Eur J Nucl Med Mol Imaging* 2018;**45**:1762–1771
10. Kunstman JW, Kirsch JD, Mahajan A, Udelsman R. Clinical review: parathyroid localization and implications for clinical management. *J Clin Endocrinol Metab* 2013;**98**:902–912
11. Paras C, Keller M, White L, Phay J, Mahadevan-Jansen A. Near-infrared autofluorescence for the detection of parathyroid glands. *J Biomed Opt* 2011;**16**:067012
12. McWade MA, Paras C, White LM, Phay JE, Mahadevan-Jansen A, Broome JT et al. A novel optical approach to intraoperative detection of parathyroid glands. *Surgery* 2013;**154**:1371–1377

13. McWade MA, Paras C, White LM, Phay JE, Solórzano CC, Broome JT et al. Label-free intraoperative parathyroid localization with near-infrared autofluorescence imaging. *J Clin Endocrinol Metab* 2014;**99**:4574–4580
14. Solórzano CC, Thomas G, Baregamian N, Mahadevan-Jansen A. Detecting the near infrared autofluorescence of the human parathyroid: hype or opportunity? *Ann Surg* 2020;**272**:973–985
15. McWade MA, Thomas G, Nguyen JQ, Sanders ME, Solórzano CC, Mahadevan-Jansen A et al. Enhancing parathyroid gland visualization using a near infrared fluorescence-based overlay imaging system. *J Am Coll Surg* 2019;**228**:730–743
16. Kose E, Kahramangil B, Aydin H, Donmez M, Berber E. Heterogeneous and low-intensity parathyroid autofluorescence: patterns suggesting hyperfunction at parathyroid exploration. *Surgery* 2019;**165**:431–437
17. Falco J, Dip F, Quadri P, de la Fuente M, Rosenthal R. Cutting edge in thyroid surgery: autofluorescence of parathyroid glands. *J Am Coll Surg* 2016;**223**:374–380
18. Collins TJ. ImageJ for microscopy. *BioTechniques* 2007;**43**:S25–S30
19. Demarchi MS, Karenovics W, Bédarid B, Triponez F. Intraoperative autofluorescence and indocyanine green angiography for the detection and preservation of parathyroid glands. *J Clin Med* 2020;**9**:830
20. Perrier ND, Ituarte P, Kikuchi S, Siperstein AE, Duh QY, Clark OH et al. Intraoperative parathyroid aspiration and parathyroid hormone assay as an alternative to frozen section for tissue identification. *World J Surg* 2000;**24**:1319–1322
21. Norman J, Politz D. 5000 parathyroid operations without frozen section or PTH assays: measuring individual parathyroid gland hormone production in real time. *Ann Surg Oncol* 2009;**16**:656–666
22. Lumachi F, Zucchetta P, Marzola MC, Boccagni P, Angelini F, Bui F et al. Advantages of combined technetium-99m-sestamibi scintigraphy and high-resolution ultrasonography in parathyroid localization: comparative study in 91 patients with primary hyperparathyroidism. *Eur J Endocrinol* 2000;**143**:755–760
23. Benmiloud F, Rebaudet S, Varoquaux A, Penaranda G, Bannier M, Denizot A et al. Impact of autofluorescence-based identification of parathyroids during total thyroidectomy on postoperative hypocalcemia: a before and after controlled study. *Surgery* 2018;**163**:23–30
24. McWade MA, Sanders ME, Broome JT, Solórzano CC, Mahadevan-Jansen A. Establishing the clinical utility of autofluorescence spectroscopy for parathyroid detection. *Surgery* 2016;**159**:193–202
25. Ladurner R, Sommerey S, Arabi NA, Hallfeldt KKJ, Stepp H, Gallwas JKS et al. Intraoperative near-infrared autofluorescence imaging of parathyroid glands. *Surg Endosc* 2017;**31**:3140–3145
26. Thomas G, McWade MA, Paras C, Mannoh EA, Sanders ME, White LM et al. Developing a clinical prototype to guide surgeons for intraoperative label-free identification of parathyroid glands in real time. *Thyroid* 2018;**28**:1517–1531
27. Serra C, Silveira L, Canudo A, Lemos MC. Parathyroid identification by autofluorescence—preliminary report on five cases of surgery for primary hyperparathyroidism. *BMC Surg* 2019;**19**:120
28. Squires MH, Jarvis R, Shirley LA, Phay JE. Intraoperative parathyroid autofluorescence detection in patients with primary hyperparathyroidism. *Ann Surg Oncol* 2019;**26**:1142–1148
29. Falco J, Dip F, Quadri P, de la Fuente M, Prunello M, Rosenthal RJ et al. Increased identification of parathyroid glands using near infrared light during thyroid and parathyroid surgery. *Surg Endosc* 2017;**31**:3737–3742